PHYSICAL REVIEW C VOLUME 23, NUMBER 4 APRIL 1981

# Inclusive scattering of protons on helium, nickel, and tantalum at 500 MeV

G. Roy, L. G. Greeniaus, G. A. Moss, D. A. Hutcheon, and R. Liljestrand
*University of Alberta, Edmonton, Alberta, Canada T6G 2N5*

R. M. Woloshyn
*TRIUMF, Vancouver, British Columbia, Canada V6T 2A3*

D. H. Boal
*Simon Fraser University, Burnaby, British Columbia, Canada V5A 1S6*

A. W. Stetz
*University of Oregon, Corvallis, Oregon 97331*

K. Aniol
*University of Washington, Seattle, Washington 98195*

A. Willis and N. Willis
*Institut de Physique Nucleaire, 91406 Orsay, France*

R. McCamis
*University of Manitoba, Winnipeg, Manitoba, Canada R3T 2N2*
(Received 26 August 1980)

We have performed proton inclusive scattering measurements at 500 MeV on $^4$He, Ni, and Ta at angles at 65°, 90°, 120°, and 160°. Analyzing powers were also obtained for $^4$He and Ni. The data extend in energy to the elastic scattering peak for $^4$He at 90°. The cross-section data are described well by a direct knockout model and by quasi-two-body scaling calculations. Fits to analyzing power results by these theories are poor, and furthermore, we find a qualitative difference between the $^4$He and Ni results. The Ni data show large positive analyzing powers at high detected particle energies, in keeping with results obtained on various targets from $^6$Li to $^{181}$Ta at 800 MeV bombarding energy; the $^4$He analyzing powers are predominantly negative or close to zero.

[NUCLEAR REACTIONS Proton inclusive scattering; $^4$He, Ni, $^{181}$Ta; $E = 500$ MeV; measured $\sigma(E_p), P(E_p)$.]

## I. INTRODUCTION

Much interest has been shown recently in large angle proton induced inclusive scattering[1-5] (i.e., $p + A \rightarrow p +$ anything) at medium and high energies. Protons observed at laboratory angles greater than 90° are in a region kinematically forbidden for free nucleon-nucleon scattering, so the fact that the target is a nucleus plays an essential role. This has been taken into account in a variety of models with different reaction mechanisms. These models include evaporation,[6] intranuclear cascade with pion production and absorption,[7] scattering from clusters in the target,[8] multinucleon exchange,[9] and scattering from a bound nucleon of high momentum.[10] All of these models can be constructed to work equally well over a limited range of energy and angle. To test them fully, data are needed over the widest possible range of energy. In this paper we present some new results for 500 MeV proton inclusive scattering obtained at the TRIUMF cyclotron. Cross sections are reported for helium, nickel, and tantalum targets. These are the first results for large angle inclusive proton production on a target as light as helium.

Previous experiments on large angle inclusive proton production have been done at incident energies of 600 MeV and higher with the most complete measurements at 800 MeV.[11] Our motivation for extending the energy down to 500 MeV is twofold. First, the cross section for pion production in nucleon-nucleon collisions changes dramatically in the 500–800 MeV range. If real pion production and absorption is a dominant mechanism for large angle proton emission,[7] we would expect to see large qualitative changes in inclusive cross sections over this energy range. Second, at 800 MeV, where the most complete measurements have been made, a scaling behavior[12] (quasi-two-body scaling) has been observed. This scaling follows as an approximation to a direct knockout mecha-

 

nism[10,13] based on a collision between the incident proton and a bound nucleon of high momentum. By going to lower energy we provide a further test of a phenomenology which has been very successful[11,13,14] in the 800 MeV region.

An important reason for extending the inclusive scattering measurements to a light nucleus such as $^4$He is to confront models based on statistical or cascade mechanisms. While these models are certainly appropriate for emission of very low energy particles, and may have some validity for high energy proton emission from heavy targets, it is unlikely that they can be applied to inclusive reactions on a nucleus as light as $^4$He. If statistical mechanisms do play an important role, we would expect to see qualitative differences between inclusive cross sections on $^4$He and $^{181}$Ta. In fact, it is already known from 800 MeV data that direct reaction models provide a unified description for cross sections from $^6$Li to $^{181}$Ta.[11,14] In this experiment we investigate an even broader target mass range.

In addition to inclusive cross sections we also measured the analyzing powers for inclusive scattering on $^4$He and Ni. $^4$He was chosen because the inclusive proton spectra could be measured right out to the elastic scattering limit; the Ni data came from the windows of the $^4$He target cell. Analyzing power data on targets from $^6$Li to $^{181}$Ta at 800 MeV (Ref. 15) have the same qualitative behavior for all targets, but we find a drastic difference between the analyzing powers of $^4$He and Ni. This may provide us with an important clue to the nature of the reaction mechanism.

In Sec. II we discuss the experimental method and data analysis. Cross sections and analyzing powers are presented for 500 MeV protons on $^4$He and Ni at laboratory angles of 65°, 90°, 120°, and 160°. For the $^{181}$Ta target, cross sections are given at angles of 90°, 120°, and 160°. In Sec. III the results are discussed within the context of the direct knockout model, and a quasi-two-body scaling analysis is presented. The conclusion is contained in Sec. IV.

## II. METHOD AND DATA ANALYSIS

Figure 1 shows a schematic of the apparatus. The scattered protons were detected in range telescopes symmetric with respect to the incoming beam. Their solid angles were approximately 5 msr. The beam polarization was continuously monitored in a beam line polarimeter. The $^4$He target was a $5\times5$ cm$^2$ by 0.77 cm cell attached to a liquid helium cryostat. The target thickness was 97 mg/cm$^2$. A dummy cell of the same size and configuration was mounted beneath the $^4$He

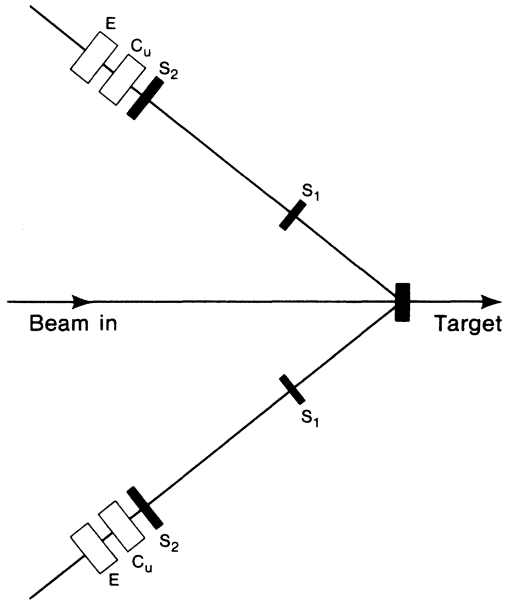


FIG. 1. Schematic of the apparatus. $S_1$ and $S_2$ are thin plastic scintillators; the $E$ detector is a 7.6 cm thick by 12.7 cm diameter NaI detector.

cell to enable the contribution of the windows of the target cell to be subtracted. Since the yield from the dummy cell was dominated by the nickel windows, we were able to obtain inclusive data for Ni with less than 10% contamination by lighter elements (predominantly oxygen and carbon). The Ni target thickness was 45 mg/cm$^2$.

The detector telescopes (left and right) consisted of two thin $\Delta E$ plastic scintillators separated by a one meter flight path to provide time-of-flight information. Following these was a copper degrader to slow down the particles and a 7.6 cm$\times$12.7 cm diameter NaI detector to provide energy information. Different thicknesses of copper absorber (0 cm, 1.9 cm, and 4.2 cm) were used to yield three overlapping scattered energy ranges from 50 to 270 MeV—the energy of elastically scattered protons from $^4$He at 90° and 500 MeV bombarding energy.

Particle identification was provided by a combination of time-of-flight and $E$-$\Delta E$ information. Figure 2 shows a typical mass identification spectrum. Although the deuterons are clearly resolved, due to kinematic limits the deuteron energies do not extend high enough to be of interest. The pions are also identifiable, but their $dE/dx$ is so small that a maximum of only ~ 65 MeV is deposited in the NaI detector, and the three energy ranges corresponding to different degrader thicknesses are small. Most of the pions pass through the NaI detector and their $E$-$\Delta E$ signature "folds

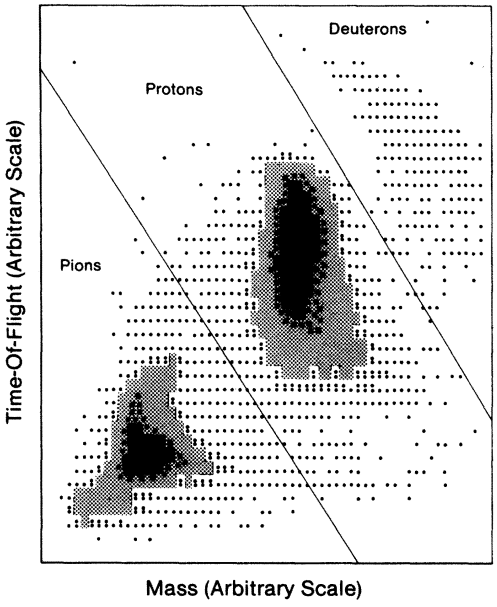


FIG. 2. Mass identification spectrum. A mass identifier obtained from the $E$ and $\Delta E$ measurements is plotted versus times of flight between $S_1$ and $S_2$.

back"; increasing pion energy yields both a smaller $\Delta E$ signal and a smaller total energy $E$ signal. Protons with energies greater than 150 MeV after the copper degrader also have this fold-back signature. There was some difficulty in separating the fold-back protons and occasional pions from stopped protons. Cuts were made on the mass identification spectra to eliminate these undesirable events. This procedure worked well at backward angles because the proton cross sections fall off rapidly with increasing energy, and pion production cross sections are small. The data at 65° were more difficult to analyze because the high energy protons become more numerous and proton fold back became a serious problem.

Inclusive scattering data are plotted in terms of the scattered energy. Therefore, in analyzing the data, a transformation from detected energy in the NaI counter to scattered energy had to be made. Large nonlinearities are introduced by the material between the target and NaI detectors. Lower energy particles lose a larger fraction of their energy in an absorber than high energy particles. Near the detection threshold a small change in detected energy corresponds to a large change in scattered energy, the scale factor being the ratio of the differential rates of energy loss at the detector and target. This ratio is large for small detected energy and approaches 1.0 asymptotically as the scattered energy increases. If data are presented on a scale which is proportional to detected energy, this effect leads to an apparent falling off in cross section at lower energies. This is the explanation for the decreasing cross sections at lower energies observed by Källne *et al.*[16] Figure 3 demonstrates this effect for 90° scattering angle on $^4$He and the three degrader thicknesses. The energy scale takes into account the average energy loss in the absorber, but the energy bins have not yet been linearized.

Figures 4–6 show the cross-section data for $^4$He, Ni, and $^{181}$Ta. The error bars indicate the degree of consistency between the left and right counters, and the consistency in the overlap regions of the three energy ranges observed at different times. The statistical errors are small compared to these potential systematic errors. The 160° $^4$He data are particularly sensitive to correction for the contribution from the target cell. Near 157 MeV (the elastic limit at 160°) the error due to background subtraction may be as large as 50%. The potential error was much smaller for the other scattering angles and is probably < 10%. The "bumpiness" in the 65° data for $^4$He and Ni is due to incomplete elimination of fold-back protons which may be as much as 10% in some regions. At the backward angles, the fold-back contamination is much smaller.

The cross-section data at all angles have the standard inclusive scattering shape—an approximately exponential falloff in the cross section with increasing scattered particle energy. This is consistent with results obtained at higher bombarding energy and backward angles. It is inter-

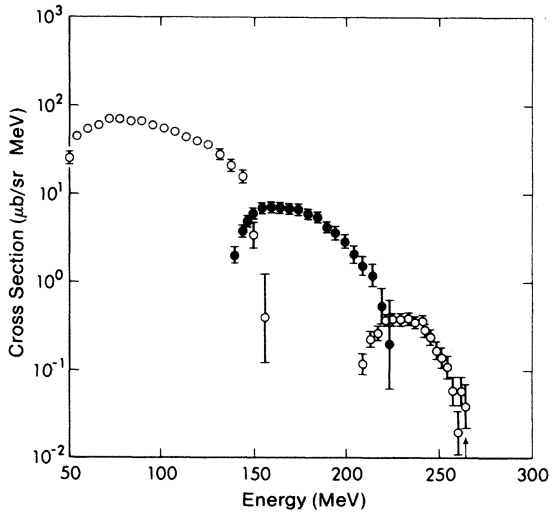


FIG. 3. $^4$He cross section data at 90°, corrected only for the average energy loss in the Cu degrader. The falloff at the start of each bite is due to the nonlinearity of the energy loss for small detected energies in the NaI detector.

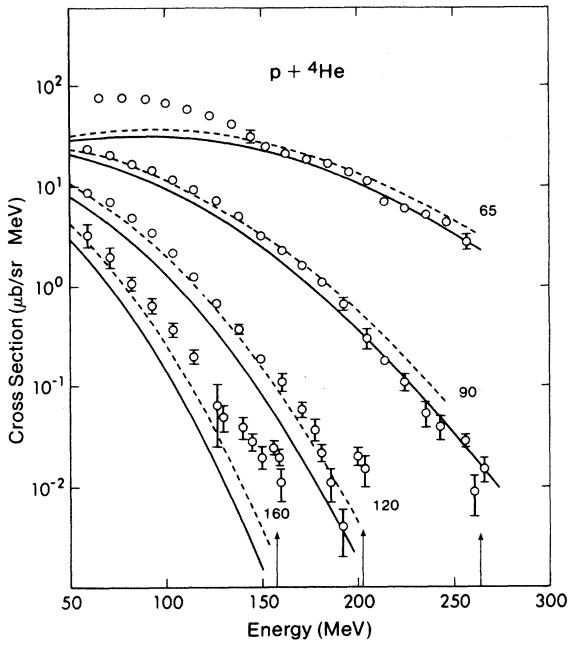


FIG. 4. $^4$He cross section data at 65°, 90°, 120°, and 160°. The arrows designate the elastic scattering energy. The solid and dashed curves are direct knockout calculations with $k_0 = 88$ and 94 MeV/$c$, respectively. Average excitation energy of the residual nucleus is zero.

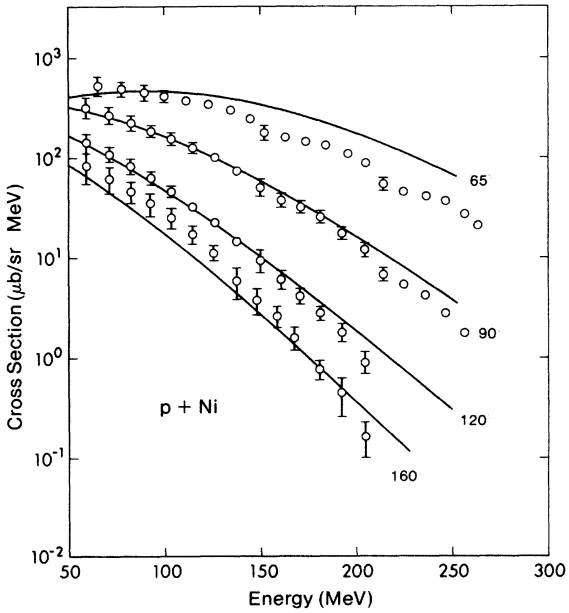


FIG. 5. Ni cross section data at 65°, 90°, 120°, and 160°. The solid curves are direct knockout calculations with $k_0 = 88$ MeV/$c$. Average excitation energy of the residual nucleus is 5 MeV.

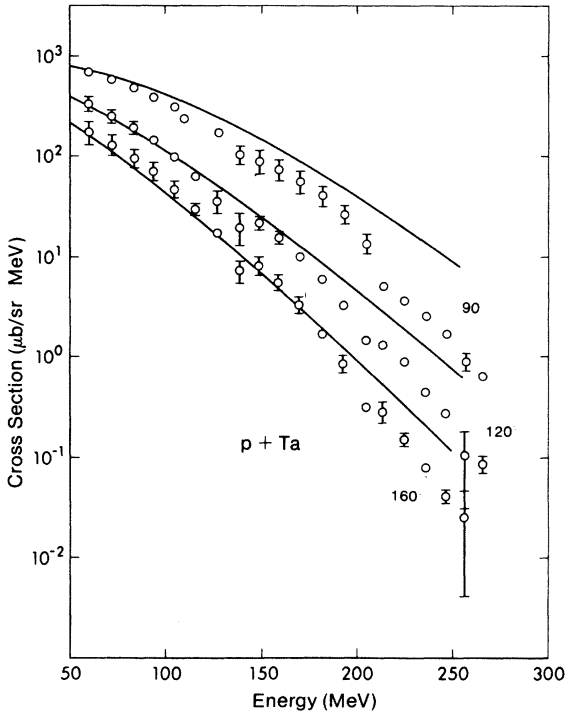


FIG. 6. Ta cross-section data at 90°, 120°, and 160°. The solid curves are direct knockout calculations with $k_0 = 88$ MeV/$c$. Average excitation energy of the residual nucleus is 15 MeV.

esting to note that this approximately exponential shape of the inclusive spectra extends out to the elastic scattering limit in $^4$He.

The polarization data are shown in Figs. 7 and 8. The errors represent statistical uncertainty in the data including effects of background subtraction. In general, analyzing powers for the left and right detectors were consistent within the statistical errors. The polarization data at 120° and 160° on both $^4$He and Ni are not much different from zero; for $^4$He, the data at 65° and 90° show small negative analyzing powers at low energies, increasing to zero with increasing energy. The 90° analyzing power remains near zero up to the elastic scattering peak. For Ni, the 65° and 90° analyzing powers start with negative values and increase to positive values with increasing energy. This behavior is similar to measurements of Frankel *et al.*[15] at 800 MeV on various nuclei heavier than $^4$He. There appears to be a fundamental difference between the $^4$He analyzing powers and those for heavier nuclei.

## III. DISCUSSION

In this paper we will emphasize the direct knockout model[13] since it has provided the most successful phenomenological description of inclusive scat-

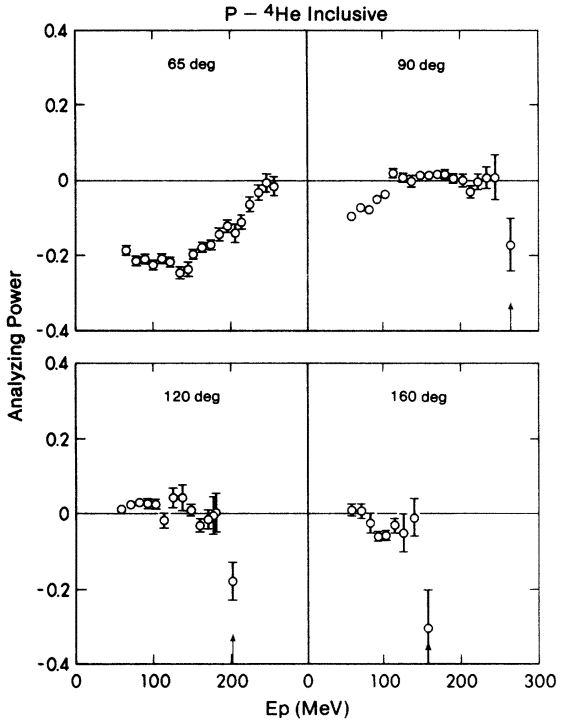


FIG. 7. $^4$He analyzing powers at 65°, 90°, 120°, and 160°. The arrows designate the elastic scattering energy. The error bars represent statistical uncertainty.

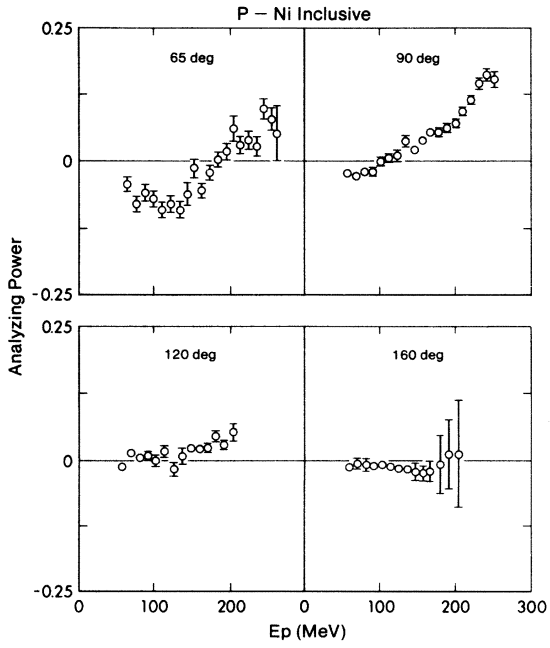


FIG. 8. Ni analyzing powers at 65°, 90°, 120°, and 160°. The error bars represent statistical uncertainty.

tering cross section at higher energies. The underlying picture is one where the incident proton scatters elastically from the observed secondary proton, the remainder of the nucleus being a spectator. Figure 9 shows this schematically and includes the kinematic labels. The $(p,p')$ differential cross section takes the form[13]

$$\frac{d^2\sigma}{d\Omega_q dE_q} = \frac{M_p{}^4}{2(2\pi)^5}\frac{q}{p_i}\int \frac{d^3p_f}{E_f\epsilon_k}[n_p(k)|T_{pp}|^2+n_n(k)|T_{pn}|^2] \times\delta(E_i+M_A-E_f-E_q-\epsilon_k), \quad (1)$$

where $\epsilon_k=(k^2+M_{A'})^{1/2}$ is the total energy of the recoiling nucleus. The closure approximation is used to replace the sum over final nuclear states with an average mass $M_{A'}$, which includes the effect of an average excitation energy of the residual nucleus. The quantities $n_p$ and $n_n$ are "momentum distributions" of the nucleons in the target nucleus and are taken to be of the form

$$n(k)=\frac{C}{[2\cosh(k/2k_0)]^2}, \quad (2)$$

where $k_0$ is a parameter and $C$ is taken from the normalization condition

$$2\int \frac{M_p}{\epsilon_k} n_p(k)\frac{d^3k}{(2\pi)^3} = Z. \quad (3)$$

$T_{pp}$ and $T_{pn}$ are related to the nucleon-nucleon scattering cross sections and are parametrized in the following fashion[13]: First, an appropriate lab kinetic energy $T_{\rm lab}$ is calculated from the Mandelstam variable $s$ defined by $p_f$ and $q$. Then $|T_{pp}|^2$ is normalized to

$$|T_{pp}|^2=\frac{16\pi p_{\rm lab}{}^2}{m_p{}^2}Ae^{bt}, \quad (4)$$

where $t$ is the Mandelstam four-momentum trans-

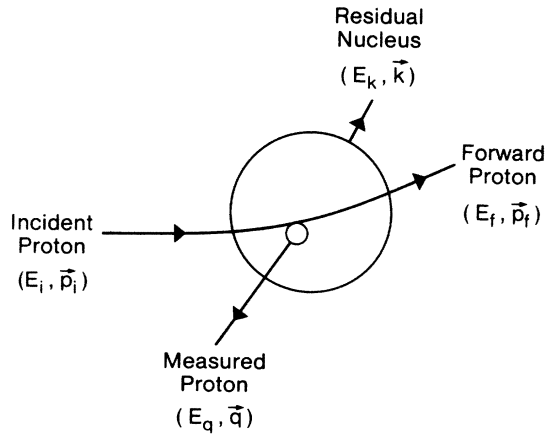


FIG. 9. Energy and momentum labels for the direct knockout process.

fer squared, $b$ is taken to be equal to $(14.39T_{\rm lab} - 6.13\ {\rm GeV}^{-2})$, and $A$ is such that the integrated $pp$ cross section is 24 mb, following Ref. 17. Equation (4) is reasonable if $b$ is limited to the range $0.7\ {\rm GeV}^{-2} < b < 7\ {\rm GeV}^{-2}$.

$T_{pn}$ can also be parametrized in a similar fashion, but since the corresponding $(p,n)$ cross sections are much smaller than the $(p,p)$ cross sections, $T_{pn}$ will contribute only a few percent of the total cross section and it is ignored.

The results of the calculations are shown in Figs. 4–6. The solid curves are calculated using a value of $k_0 = 88$ MeV/$c$. This $k_0$ value was also found[13] to fit the 800 MeV data quite well. The dashed curves fitting the helium data were calculated using $k_0 = 94$ MeV/$c$. Increasing $k_0$ simply increases the calculated cross sections, but the shapes of the curves hardly change. The mass of the residual nucleus $M_{A'}$ includes an average excitation energy which was chosen to be 0, 5, and 15 MeV for $^4$He, Ni, and Ta, respectively. Again the effect of a different excitation energy is to change the magnitude of the cross section, but not the shape. Note that the back-angle data for all targets are fitted quite well, but the 65° data are not, although the trend of the cross sections is followed.

It must be admitted that $k_0$ and the average excitation energy of the residual nucleus cover a multitude of omissions in the model—final state interactions, meson exchange effects, etc. Hence it is surprising that the same (or similar) value of $k_0$ can be used to fit the absolute magnitudes of such a wide range of experimental data at different bombarding energies, targets, and angles. Because we do not expect statistical mechanisms to be important for the $^4$He target, these analyses imply that the same (or slightly modified) direct mechanisms apply for both $^4$He and a heavier target.

For a rapidly falling structure function $n(k)$ the elastic amplitude can be factored outside the integral (1) and the integral will be dominated by the minimum value of recoil momentum $k_{\rm min}$.[12] The inclusive cross section can be written as

$$\frac{d^2\sigma}{d\Omega_q dE_q} = \frac{C(p,k_{\rm min})}{|\vec{p}_i - \vec{q}|} G(k_{\rm min}) \qquad (5)$$

where

$$C(p,k_{\rm min}) = \frac{s(s-4m_p^2)}{32\pi^2 p m_p E_q} \frac{d\sigma}{dt}\,(\vec{k}_{\rm min} \to \vec{q}) \qquad (6)$$

and $s$ and $t$ are the appropriate Mandelstam variables, and $(d\sigma/dt)(\vec{k}_{\rm min} \to \vec{q})$ is the nucleon-nucleon cross section evaluated using the same parametrization as in the direct knockout model. $G(k_{\rm min})$ is a universal structure function and contains the momentum distribution of the nucleons in the target nucleus. This is Frankel's quasi-two-body-scaling (QTBS) hypothesis.[12] It has been previously verified for inclusive scattering on targets ranging from $^6$Li to $^{181}$Ta at 800 MeV bombarding energy.[11,14] Figures 10–12 are plots of $G(k_{\rm min})$ versus $k_{\rm min}$ for $^4$He, Ni, and $^{181}$Ta at 500 MeV bombarding energy. QTBS is very well satisfied by the Ni and $^{181}$Ta data and fairly well satisfied for $^4$He, over a large range of $k_{\rm min}$. The straight lines are least squares fits to the data and correspond to a momentum distribution of the form $\exp(k/k_0)$.

Figure 13 is a plot of $G(k_{\rm min})$ per nucleon for all our data. The Ni and $^{181}$Ta data can be fit reasonably by one structure function, but the $^4$He results deviate from the other data, particularly at high values of $k_{\rm min}$. Frankel *et al.*[2] were able to fit data from $^6$Li to $^{181}$Ta with one structure function; our result again shows a distinct difference between $^4$He and heavier nuclei.

Analyzing powers for QTBS can be estimated by using the nucleon-nucleon analyzing power at the appropriate effective lab kinetic energy and angle.[18] The analyzing powers predicted in this fashion are shown in Fig. 14 for $^4$He. It is clear that the QTBS predictions are considerably more negative than experiment. Analyzing powers for the direct knockout model can be estimated in a similar way, but since this model integrates over

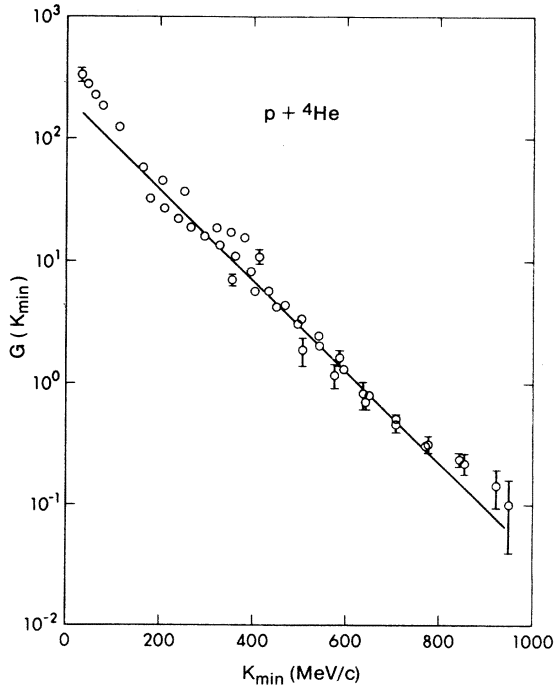


FIG. 10. Plot of $G(k_{\rm min})$ vs $k_{\rm min}$ for all of the $^4$He data. The slope of the straight line corresponds to $k_0 = 109$ MeV/$c$.

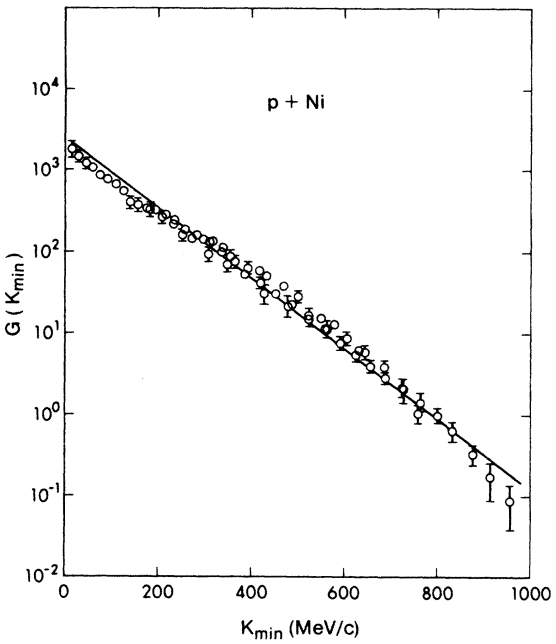


FIG. 11. Plot of $G(k_{min})$ vs $k_{min}$ for all of the Ni data. The slope of the straight line corresponds to $k_0 = 103$ MeV/$c$.

a range of internal momentum $k$, a suitable range of nucleon-nucleon analyzing powers is included. The predictions will be smaller in magnitude than those for QTBS, particularly for large and small angle scattering. The 90° results will not change much. However, even including the proper inte-

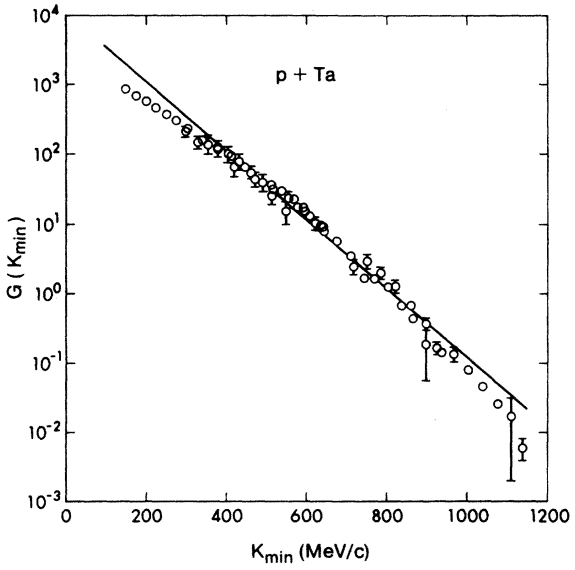


FIG. 12. Plot of $G(k_{min})$ vs $k_{min}$ for all of the Ta data. The slope of the straight line corresponds to $k_0 = 89$ MeV/$c$.

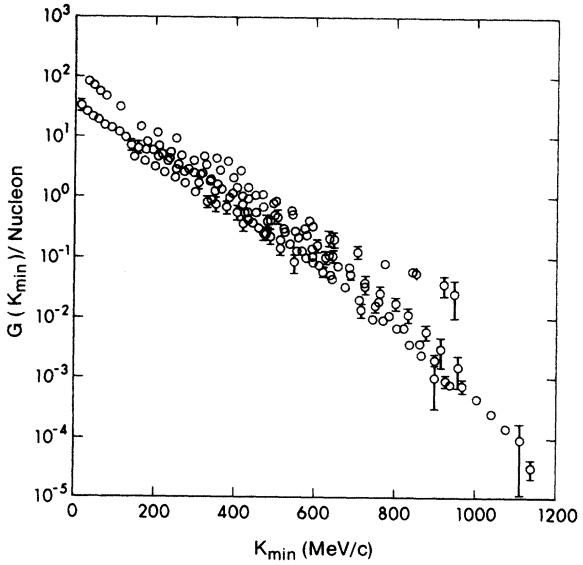


FIG. 13. Plot of $G(k_{min})/A$ vs $k_{min}$ for all targets.

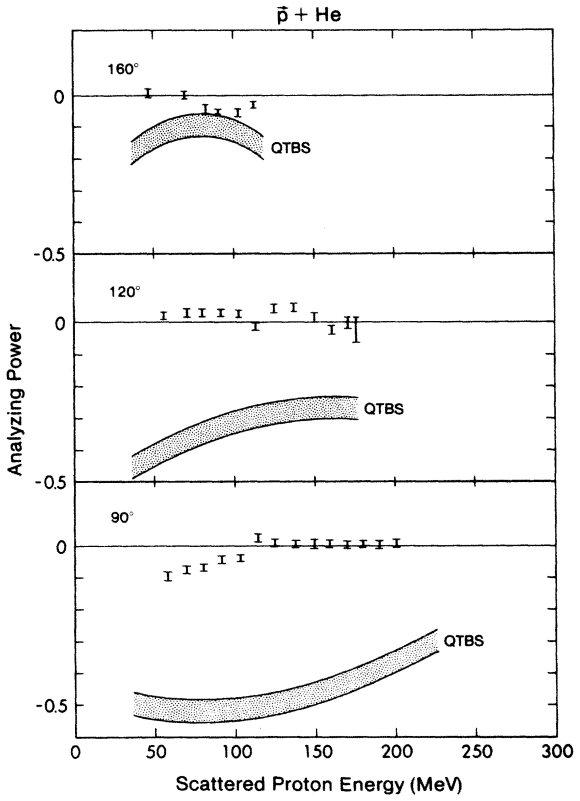


FIG. 14. $^4$He analyzing power compared with QTBS predictions. The band represents the theoretical calculations.

gration, the positive analyzing powers observed in the Ni data cannot be obtained from a direct knockout model with an on-shell $p$-$p$ amplitude.

## IV. CONCLUSIONS

In this paper we report results for inclusive proton scattering at 500 MeV on $^4$He, Ni, and $^{181}$Ta. We show that:

(i) A direct knockout model previously used at 800 MeV provides a good quantitative description of our 500 MeV data, implying that the reaction mechanism is not changing over this energy range. This suggests large angle proton emission is not directly related to the nucleon-nucleon pion production cross section which changes drastically from 500–800 MeV.

(ii) The quasi-two-body-scaling hypothesis is satisfied at 500 MeV just as it is at 800 MeV. The scaling function $G(k_{\min})$ for Ni and $^{181}$Ta is very similar to the universal scaling function obtained by Frankel *et al.*[11] at 800 MeV. QTBS is less well satisfied by the $^4$He data.

(iii) The analyzing power of 500 MeV inclusive scattering on Ni becomes positive at large values of the observed proton energy and is qualitatively similar to results at 800 MeV. The analyzing power for the $^4$He target is small for angles $> 90°$ and does not approach the elastic scattering analyzing power in a continuous way. The analyzing power for $^4$He or Ni cannot be explained by QTBS or the direct knockout model in which the primary interaction is assumed to be $pp$ scattering.

If one takes the high momentum component of the wave function in the direct knockout model seriously, then the incident proton is really scattering off a composite object, rather than a free proton. Both the $p$-$^4$He and $p$-$d$ reactions show a change in sign of the analyzing power at significantly smaller angles than $pp$ scattering in the 200–500 MeV kinetic energy range. While this may account for the lack of large negative analyzing powers in the $^4$He data at 90°, the Ni data are very likely showing evidence of multiple scattering.

However, it is probable that the analyzing power results will be more sensitive to multiple scattering effects than the inclusive cross section. The effect of multiple scattering on the differential cross section will be to make it more isotropic, although this effect should not be too large because the $p$-nucleon and $p$-nucleus elastic scattering amplitudes are all peaked at $t = 0$. Further evidence for the lack of a strong dependence of the cross section on multiple scattering comes from its target dependence. For emitted proton energies in the 100 MeV range, the differential cross section increases roughly as $A$, while in the 300 MeV range it goes roughly as $A^{1.6}$, certainly less than expected if multiple scattering were playing a dominant role.

## ACKNOWLEDGMENTS

We would like to express our thanks to C. A. Miller and H. Coombes who helped with the electronics during the experiment, and to J. Arvieux for help with the data taking. This work was supported in part by the Natural Sciences and Engineering Council of Canada.

[1] D. R. F. Cochran, P. N. Dean, P. A. M. Gram, E. A. Knapp, E. R. Martin, D. E. Nagle, R. B. Perkins, W. J. Schlaer, H. A. Thiessen, and E. D. Therist, Phys. Rev. D 6, 3085 (1972).
[2] S. Frankel, O. Van Dyck, V. Highland, W. Frati, and R. Werbeck, Phys. Rev. Lett. 36, 642 (1976).
[3] H. Brody, S. Frankel, W. Frati, D. Yang, C. F. Perdrisat, J. C. Comiso, and K. O. H. Ziock, Phys. Lett. 71B, 79 (1977).
[4] J. P. Alard, A. Baldit, R. Brun, J. P. Costilhea, J. Dhermain, J. Fargeix, L. Fraysse, J. Pellet, G. Roche, J. C. Tamain, and A. Cordaillat, Nuovo Cimento 30A, 320 (1975).
[5] V. I. Komarov, G. E. Kosarev, H. Muller, D. Netzband, and T. Stiehler, Phys. Lett. 69B, 37 (1977).
[6] T. F. Hoang, Phys. Rev. D 15, 2533 (1977).
[7] V. I. Komorov, G. E. Kosarev, H. Muller, D. Netzband, V. D. Toneev, T. Stiehler, S. Tesch, K. K. Gudina, and S. G. Mashnik, Nucl. Phys. A326, 297 (1979).
[8] T. Fujita, Phys. Rev. Lett. 39, 174 (1977).
[9] H. J. Weber and L. J. Miller, Phys. Rev. C 16, 726 (1977).
[10] R. D. Amado and R. M. Woloshyn, Phys. Rev. Lett. 36, 1435 (1976).
[11] S. Frankel, W. Frati, G. Blanpied, G. W. Hoffmann, T. Kozlowski, C. Morris, H. A. Thiessen, O. Van Dyck, R. Ridge, and C. Whitten, Phys. Rev. C 18, 1375 (1978).
[12] S. Frankel, Phys. Rev. Lett. 38, 1338 (1977).
[13] D. H. Boal, Phys. Rev. C 21, 1913 (1980).
[14] S. Frankel, W. Frati, R. M. Woloshyn, and D. Yang, Phys. Rev. C 18, 1379 (1978).
[15] S. Frankel, W. Frati, M. Gazzaly, G. W. Hoffmann, O. Van Dyck, and R. M. Woloshyn, Phys. Rev. Lett. 41, 148 (1978).
[16] J. Källne, A. W. Stetz, and R. M. Woloshyn, Phys. Lett. 74B, 170 (1978).
[17] Particle Data Group, Lawrence Radiation Laboratory, Berkeley, 1970, Report No. UCRL 20000NN (unpublished).
[18] S. Frankel and R. M. Woloshyn, Phys. Rev. C 16, 1680 (1977).

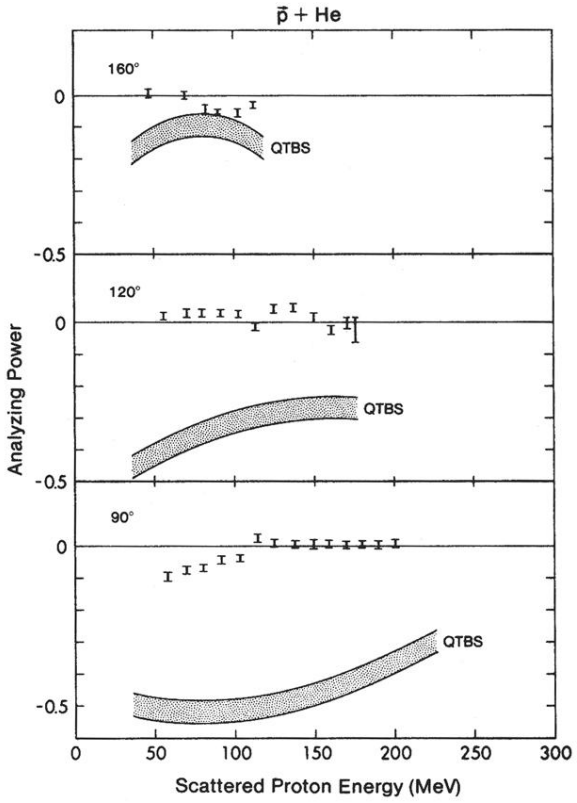


FIG. 14. $^4$He analyzing power compared with QTBS predictions. The band represents the theoretical calculations.

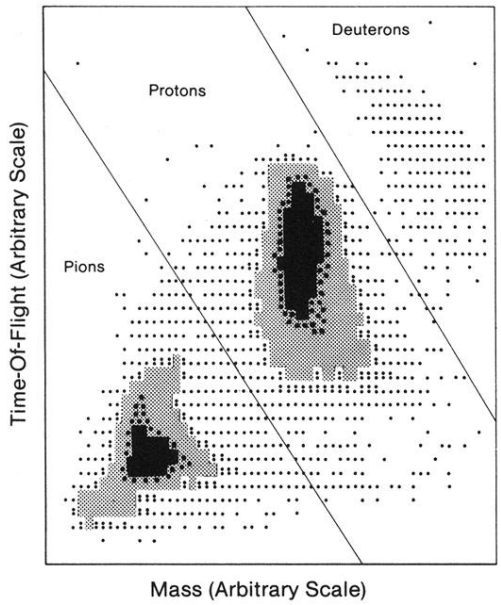


FIG. 2. Mass identification spectrum. A mass identifier obtained from the $E$ and $\Delta E$ measurements is plotted versus times of flight between $S_1$ and $S_2$.